



The effects of precursory velocity changes on earthquake nucleation and stress evolution in dynamic earthquake cycle simulations

Prithvi Thakur ^{a,b,*}, Yihe Huang ^b

^a Brown University, Center for Computation and Visualization, 180 George Street, Providence, 02919, RI, USA

^b University of Michigan, Department of Earth and Environmental Sciences, 1100 North University Building, Ann Arbor, 48109, MI, USA



ARTICLE INFO

Editor: R. Bendick

Keywords:

earthquake cycles
velocity precursors
fault damage zone
slow-slip

ABSTRACT

Seismic velocity changes in earthquake cycles have been observed over a wide range of timescales and may be a good indicator of the onset of future earthquakes. Understanding the effects of precursory velocity changes right before seismic and slow-slip events could potentially elucidate the onset and timing of fault failure. We use numerical models to simulate fully dynamic earthquake cycles in 2D strike-slip fault systems with antiplane geometry, surrounded by a narrow fault-parallel damage zone. By imposing S-wave velocity changes inside fault damage zones, we investigate the effects of these precursors on multiple stages of the seismic cycle, including nucleation, coseismic, postseismic, and interseismic stages. Our modeling results show a wide spectrum of fault slip behaviors including fast earthquakes, slow-slip events, and variable creep. One primary effect of the imposed velocity precursor is on the earthquake nucleation phase, and earlier onset of precursors causes earthquakes to nucleate sooner with a smaller nucleation size that is not predicted by theoretical equations. Furthermore, such precursors affect the nucleation of dynamic earthquakes and slow-slip events. Our results highlight the importance of short- and long-term monitoring of fault zone structures for better assessment of regional seismic hazard.

1. Introduction

Earthquakes are a complex phenomenon occurring over a wide range of spatial and temporal scales. They are believed to result from a sudden release of accumulated energy manifested either as failure in intact rocks or sudden stick-slip motion on preexisting faults. Understanding the onset and timing of fault failure leading to earthquakes is one of the ultimate goals of seismology. The seismic cycle consists of several distinct phases: preseismic, seismic, and postseismic, and interseismic (Scholz, 1998). The preseismic phase refers to the period leading up to an earthquake, characterized by the acceleration of creep, build-up to earthquake nucleation, and the subsequent failure resulting in dynamic ruptures, i.e., the seismic phase. The postseismic phase follows the earthquake with a period of stress relaxation and inelastic deformation. The interseismic phase is primarily associated with a locked fault, where the tectonic plate loading results in gradual stress buildup. Earthquake nucleation refers to the initial stage of an earthquake's development, where a fault evolves from a locked state to one where slip acceleration occurs. During nucleation, the stress within the

Earth's crust surpasses the strength of the rocks restraining it, leading to the initiation of fault movement (Lapusta and Rice, 2003; Ellsworth and Beroza, 1995). As the fault slips and seismic energy is released, this marks the beginning of the earthquake rupture. Nucleation is a critical phase in understanding earthquake processes, and studying it provides insights into the factors that influence the timing, location, and magnitude of earthquakes. However, our current understanding of the earthquake preparation processes, including the nucleation phase that leads to the start of earthquake rupture acceleration, is still limited. By investigating the factors that contribute to earthquake nucleation, such as precursor phenomena, fault properties, and stress changes, we can gain insights into the fundamental processes that control earthquake initiation and propagation. Earthquake precursor phenomena are unusual events or changes in the fault zone's properties, including the fault's geometry, rigidity, composition, and the presence of fluids (Cicerone et al., 2009). Their changes can be manifested as stress changes, opening and closure of microcracks, and fluid variations that occur before an earthquake. In this study, we focus on the precursory velocity changes resulting from change in fault zone rigidity and

* Corresponding author.

E-mail addresses: prithvi_thakur@brown.edu, prith@umich.edu (P. Thakur).

how they affect earthquake nucleation and stressing history in seismic cycles.

The observations of preseismic signals in natural faults include the reduction in b-values prior to large earthquakes and slow-slip events leading up to large earthquakes, e.g., the 2011 Mw 9.0 Tohoku-Oki earthquake (Kato et al., 2012; Nanjo et al., 2012; Ito et al., 2015), and the 2014 Mw 8.1 Iquique, Chile earthquake (Kato and Nakagawa, 2014). b-values are a measure of number of large earthquakes in relation to number of smaller earthquakes along a given fault. (Kato et al., 2012) identified a large number of very small, repeating earthquakes prior to the Tohoku earthquake that migrated through time slowly towards the mainshock hypocenter. This study suggests that two slow-slip transient sequences propagated towards the initial rupture point of the large Tohoku earthquake. Similar observations were documented prior to the large Iquique earthquake (Kato and Nakagawa, 2014). Additionally, changes in seismic wave velocity have been observed along natural faults prior to earthquakes (Whitcomb et al., 1973; Niu et al., 2008; Chiarabba et al., 2020). Whitcomb et al. (1973) found that both the P- and S-wave velocities significantly decreased, with $\frac{V_p}{V_s}$ decreasing by 10%, about 3.5 yrs before the 1971 San Fernando earthquake followed by a slower recovery period. Niu et al. (2008) observed precursory velocity changes approximately 10 and 2 hours prior to two earthquakes using the travel time data from active source experiments in the SAFOD drill site.

The observations of precursors are challenging to detect regularly, however, precursory signals have been observed and documented in laboratory fault experiments. Scuderi et al. (2016) have studied such robust precursory signals in laboratory fault experiments and found systematic reduction in seismic wave velocities by 1% during fast earthquakes and 3% during slow earthquakes, which are both believed to start via the same nucleation process (Kato et al., 2012; Bouchon et al., 2013; Hulbert et al., 2019). The mechanisms for these precursory seismic velocity changes are primarily attributed to the accelerating fault deformation, fluid effects, and opening and closure of microcracks due to stress changes (Scuderi et al., 2016; Poli, 2017; Stanchits et al., 2003; Rivet et al., 2016). Scuderi et al. (2016) showed that during the preseismic phase, creep begins to accelerate and marks the onset of nonlinear elastic deformation, in which the material response to stress is nonlinear with respect to strain, but the material still returns to its original shape. Such nonlinear elastic deformation is commonly used to model fault-slip while preserving the elasticity of the host rock. Fault creep and V_p reduction in lab experiments indicate that asperity contacts within the fault zone begin to fail before macroscopic frictional sliding. However, how such velocity precursors may impact the earthquake rupture and nucleation process is largely unknown. Here, we aim to investigate the potential of precursory velocity changes as an indicator of earthquake size, onset, and duration. Specifically, we aim to explore how the duration of such velocity precursors may impact the earthquake nucleation and rupture process.

Observations of preseismic signals in natural faults reveal distinctive features related to both precursory fault slip behavior and variations in physical rock properties. Natural faults are often surrounded by a network of fractures with multi-scale localization of deformation, and referred to as a fault damage zone (Lewis and Ben-Zion, 2010; Yang et al., 2011; Niu et al., 2008). Numerical models of earthquakes in fault damage zones approximated as elastic low-velocity layers suggested that they can influence dynamic rupture styles (Huang and Ampuero, 2011; Huang et al., 2014) as well as long-term seismic cycle behaviors (Abdelmeguid et al., 2019; Thakur et al., 2020; Nie and Barbot, 2021). Additionally, these fault damage zones may change in elastic strength throughout the earthquake cycle due to coseismic damage accumulation and interseismic healing (Thakur and Huang, 2021, and references therein), which give rise to variability in earthquake size, location, and interevent times in immature and mature fault zones.

Such changes in elastic strength can also lead to permanent deformation, that can occur in fault zones via a suite of mechanisms (Sibson,

1977). One such mechanism is the development of localized shear bands or faults that result from the accumulation of strain and stress concentration within the damage zone. These localized faults can propagate through the rock mass, resulting in slip and displacement across the fault zone. Another mechanism is the formation of compaction bands, which are narrow zones of high deformation within the damage zone. Compaction bands result from the localized compression of the rock mass and can lead to significant permanent deformation and reduction in the permeability of the rock (Cox and Scholz, 1995). Fracture propagation and coalescence can also contribute to permanent deformation in earthquake fault damage zones (Mendecki and Chester, 2000). This occurs when fractures in the rock mass grow and merge, resulting in the formation of larger and interconnected fractures. The propagation and coalescence of fractures can lead to significant displacement and deformation in the rock mass. Overall, the mechanisms for internal faulting and permanent deformation in earthquake fault damage zones are complex and can be influenced by a variety of factors, including rock properties, stress conditions, and the nature and intensity of seismic activity. We have chosen to model the fault zone deformation in a purely elastic sense, with time-dependent healing only occurring during quasi-static phase.

The fault-slip behavior over multiple earthquake cycles is also governed by other factors including the variation of initial stress at different scales (Andrews and Ma, 2016) as well as the earthquake nucleation size and duration (Lapusta and Rice, 2003; Cattania, 2019). The distribution of initial shear stress plays a crucial role in determining the static and dynamic stress change on the fault plane and the associated energy release and seismic radiation during an earthquake. Dynamic rupture models with heterogeneous power-law stress distribution, i.e., non-uniform self-similar distribution along depth, have partially explained the observed scaling of stress drop, moment, and radiated motion (Ripperger et al., 2007; Andrews and Barall, 2011; Dalguer and Mai, 2011). Models simulating the whole earthquake cycle (Tal and Hager, 2018; Tal et al., 2018; Ozawa et al., 2019) also utilize the spatial roughness of faults to induce stress heterogeneities. Therefore, it is evident that both stress and material heterogeneities play important roles in the generation mechanisms of earthquakes in natural fault zones.

Understanding the interplay between stress conditions, near source deformation and fault-slip heterogeneities is crucial for gaining insights into fault behavior and earthquake dynamics. Our modeling approach simplifies the fault zone deformation to a purely elastic sense, and we discuss the effects of precursory velocity changes on earthquake cycle dynamics in this study. We model the precursory velocity changes as transient, interseismic changes in damage zone rigidity to study its effects on nucleation and dynamics of subsequent ruptures. Since a natural fault rarely has uniform background stresses, we also show the effects of such precursory velocity changes in earthquake cycles on a fault with a self-similar distribution of initial normal stress with depth, which may manifest due to a priori stress heterogeneities, local geologic structures, or stress transfer from surrounding faults. Our results show that the onset of precursory shear wave velocity-drop causes a reduction in earthquake nucleation size, with earlier precursors showing smaller nucleation size. We also see that such precursory velocity changes cause earlier nucleation of earthquakes, therefore causing a reduction in recurrence intervals over the seismic cycle. Additionally, precursory velocity changes allow some intermediate magnitude earthquakes, that do not break through the entire fault asperity, to grow into full ruptures spanning the entire fault width. We also discuss how the heterogeneities in shear stress after multiple earthquakes along a fault are manifested due to fault damage zones, precursors, as well as initial self-similar normal stress.

2. Methods

We use physics-based numerical models to simulate dynamic earthquake cycles in a two-dimensional vertical strike-slip fault with an-

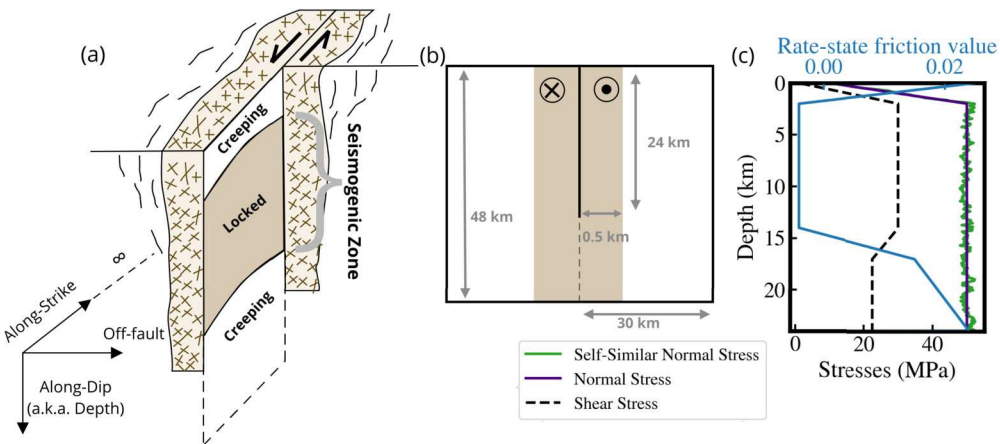


Fig. 1. Model description and setup. (a) A schematic fault damage zone along a strike-slip fault. (b) The model geometry for our numerical simulation. It represents a vertical cross-section across the fault zone schematic in Fig. 1a, with a fixed fault damage zone width. The model is infinite along strike. (c) The initial stresses and friction parameters along the fault depth.

tiplane geometry. Our modeling covers all stages, employing a 2D spectral element method (Kaneko et al., 2011, and references therein). For simplicity, we represent the fault-parallel damage zone with a constant-geometry layer. The material is purely elastic, with the damage zone having a lower shear modulus. Initial conditions are depth-dependent on an antiplane fault, without along-strike variable properties. Full inertial effects with explicit time-stepping are considered during dynamic ruptures, while a quasi-static algorithm with implicit adaptive time-stepping is used during the interseismic period (Lapusta et al., 2000).

2.1. Model setup

Our model domain extends to 48 km in depth and 30 km in width (Fig. 1b). Since this setup is symmetric across the fault, we only consider one half of the domain to save computational cost. The top boundary represents the earth's free-surface and is therefore imposed to be stress-free. The fault zone boundary is divided into two parts: the top 24 km of the boundary is the active fault governed by rate- and state-dependent friction laws, and the bottom 24 km loads the fault with a constant velocity of 35 mm yr^{-1} . The other boundaries are absorbing boundaries that allow seismic waves to pass through. The seismogenic zone, a segment of the fault that accumulates stress during the interseismic period to eventually host earthquakes, extends from 2 km to 17 km along the fault as in typical strike-slip fault systems. The rest of the fault creeps aseismically. The characterization of faults into seismic failure or aseismic creep is done based on the rate- and state-dependent friction parameter ($a - b$), with a negative value specifying a seismically active locked fault, and a positive value specifying aseismic stable sliding (Blanpied et al., 1991). Mature fault damage zones in our simulations are approximated as elastic layers parallel to the fault with lower shear moduli than the surrounding host rock. The damage zone is 1 km wide and extends throughout the domain of the simulation. The host rock has a density of 2670 kg/m^3 and an S-wave velocity of 3464 m s^{-1} . The damage zone has a density of 2670 kg/m^3 and an S-wave velocity of 2425 m s^{-1} , implying a 30% velocity reduction, similar to what is observed in nature for mature strike-slip fault zones (Huang et al., 2014; Perrin et al., 2016; Thakur et al., 2020).

The nucleation phase typically involves a gradual increase in slip rate, reflecting the accumulation of stress on the fault until it reaches a critical point, leading to rapid slip and the onset of an earthquake. In the context of numerical models of seismic cycles, we switch 'on' inertial effects as the maximum fault slip-rate increases after certain threshold, 1 mm/sec in this case (Lapusta and Rice, 2003). The onset of earthquakes in our models is captured when the peak slip-rate of the fault exceeds 1 mm/sec. We prescribe the precursory velocity drop δV_s

during the nucleation phase when the fault-slip starts accelerating. This is in-part due to the scope of this article to understand the effects of such δV_s change on earthquake nucleation, but also to make our purely elastic models thermodynamically consistent by only prescribing δV_s during the quasi-static phase, i.e., the absence of inertial effects.

2.2. Friction laws

The laboratory-derived rate- and state-dependent friction laws determine how fast the fault is slipping in relation to the shear strength (Dieterich, 1979; Ruina, 1983; Blanpied et al., 1991). We use a regularized version of the classic rate- and state-dependent friction, wherein the regularization is interpreted as a thermally activated creep model that relates the shear strength (T) to the slip rate ($\dot{\delta}$) as follows:

$$T = a\bar{\sigma} \operatorname{arcsinh} \left[\frac{\dot{\delta}}{2\dot{\delta}_0} e^{\frac{f_0 + b\ln(\dot{\delta}\theta/L)}{a}} \right] \quad (1)$$

where $\bar{\sigma}$ is the effective normal stress (the difference between lithostatic stress and the pore fluid pressure), f_0 is a reference friction coefficient corresponding to a reference slip-rate $\dot{\delta}_0$, and a and b are empirical constants that depend on the mechanical and thermal properties of the interface in contact. The parameter θ is a state variable interpreted as the average lifetime of the surface in contact and L_c is the characteristic length scale over which the contact surface slips. The evolution of the state variable is governed by the aging law (Ruina, 1983):

$$\frac{d\theta}{dt} = 1 - \frac{\dot{\delta}\theta}{L} \quad (2)$$

The frictional stability on the fault is determined by the parameter ($a - b$). Fig. 1c shows the depth profile for the friction parameter ($a - b$). The seismogenic zone (2 km to 17 km) is prescribed to be velocity weakening at steady state, which means it has potential to develop unstable slip. The rest of the fault is prescribed to be velocity strengthening at steady state, implying a stable sliding behavior. This profile is similar to what is expected at equivalent depths from laboratory and numerical experiments (Blanpied et al., 1991; Lapusta et al., 2000). Earthquake dynamics are determined by the parameters a/b and L_c . A lower value of L_c relative to the size of the velocity weakening asperity results in more chaotic rupture styles (Cattania, 2019; Barbot, 2019), whereas a/b controls the relative importance of strengthening and weakening effects and the ratio of static to dynamic stress drops (Barbot, 2019).

The region where the shear resistance breaks down at the rupture front is described as the cohesive zone (Rubin and Ampuero, 2005). The nucleation length and the cohesive zone size can have important effects on the spatiotemporal patterns of fault-slip behavior and need to be well resolved (Rubin and Ampuero, 2005; Erickson et al., 2020). We set

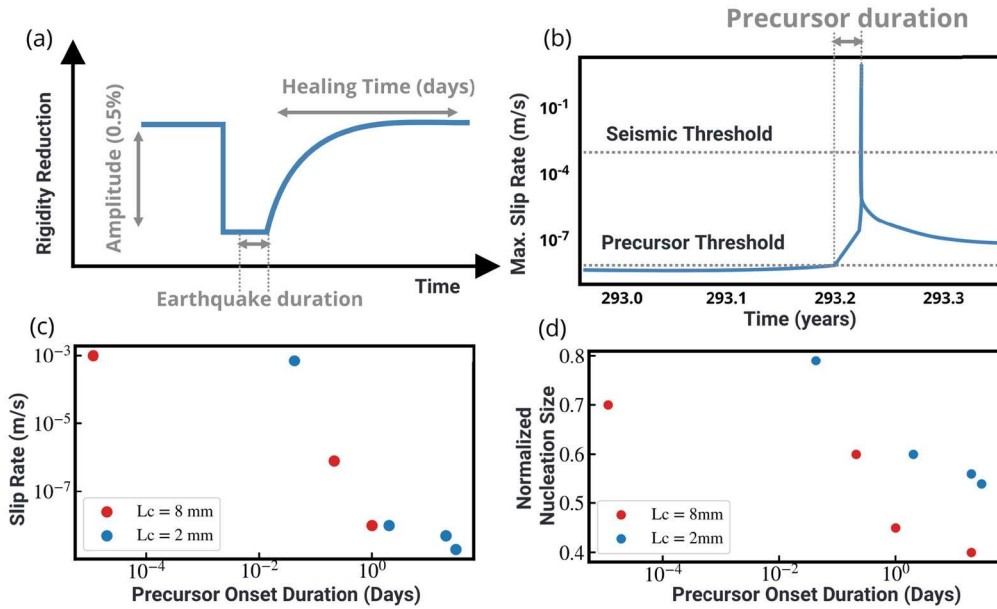


Fig. 2. Precursor setup and simulation parameters. (a) The rigidity evolution with time showing the setup of precursory velocity change. (b) A representative earthquake from our simulations highlighting the onset of precursory velocity reduction given a seismic slip-rate threshold. (c) Slip-rate thresholds used in our simulations to set up precursor durations. (d) Observed nucleation size which is normalized against the theoretical estimates is shown for the different precursor onset duration.

$L_c = 2$ mm in our first set of results (Sections 3.1-3.3) which implies an approximate nucleation size of 500 m within the damage zone. We use an average spatial resolution of 33 m, which ensures that we have more than 15 elements within the nucleating region and that the simulations are well resolved (Thakur et al., 2020). Additionally, we show another set of results in Section 3.4 with $L_c = 8$ mm in order to understand the effects of precursory velocity changes in earthquake cycles with full, periodic ruptures. All the parameters used for our simulations are described in Table A.1.

3. Results

3.1. Precursory velocity change and its effects on nucleation size

We model the velocity precursor as changes in the S-wave velocity of the fault damage zone surrounding a strike-slip fault. While the laboratory experiments have documented a change in the P-wave velocity (Scuderi et al., 2016), natural faults often show equivalent changes in P- and S-wave velocities in the absence of fluid effects (Whitcomb et al., 1973; Thurber et al., 2003). Our models are two-dimensional and under antiplane strain approximation, and therefore the models only have SH waves and we assume that similar changes in material properties during the nucleation phase would lead to SH wave velocity reduction as well. Since fully dynamic earthquake cycle models do not provide any constraint on the earthquake location and timing except the initial stress and friction values, we use the maximum slip velocity on the fault as a threshold for prescribing the precursory velocity-drop (Fig. 2). Once the on-fault slip-rate exceeds the threshold, the S-wave velocity drops instantaneously by 0.5 %. It is imperative to note that this drop happens only within the fault damage zone, where the S-wave velocity is already 30 % lower than the surrounding host rock. Once the earthquake has completely ruptured and the on-fault acceleration reaches 0, the fault zone is set up to heal back to its original value logarithmically with time. Such logarithmic healing has been observed in natural fault zones (Niu et al., 2008; Vidale and Li, 2003) and laboratory experiments (Shreedharan et al., 2020). This healing happens over 21 days in our models, which is chosen to be short enough so that it does not affect the subsequent earthquakes in the sequence (Fig. 2a). Hereafter, we refer to the shear wave velocity change as δV_s , with increase referring to

damage reduction and decrease referring to healing. The evolution of the shear wave velocity, and hence the shear modulus in the fault damage zone (μ_D) with respect to the shear modulus of the host rock (μ) is given as follows:

$$\frac{\mu_D}{\mu} = \begin{cases} \frac{\mu_D}{\mu_0}, & \text{if } V_{max} \geq V_{threshold} \\ (1 - \exp(-r(t - t_{start}))) + A_0, & \text{if } \frac{\mu_D}{\mu} < A_0 \end{cases} \quad (3)$$

where A_0 is the specified amplitude of the shear modulus change corresponding to δV_s , r is the healing rate, and $t - t_{start}$ is the timestep relative to the previous earthquake. δV_s increase starts after the current earthquake is over, while t_{start} refers to the start time of that earthquake. Each simulation shown in the subsequent sections represents two model runs, one for estimating the precursor duration given the velocity threshold, and another with the known precursor duration.

The evolution of on-fault peak slip-rate with time is indicative of the precursor onset duration (Fig. 2b). We can observe a sharp log-linear acceleration of fault-slip rate due to this δV_s . It is important to note that the actual duration of precursor prior to an earthquake does not have a strict relation to the slip-rate threshold we use, and the duration needs to be calculated after running the simulations. A lower slip-rate threshold leads to a longer precursor duration because in an ideal, homogeneous material, slip-rate increases logarithmically with time as a rupture nucleates (Lapusta and Rice, 2003). The measured precursor durations suggest a logarithmic relationship with the precursor slip-rate threshold for $L_c = 2$ mm and $L_c = 8$ mm (Fig. 2c), but more data points are needed to establish a quantitative relationship.

We also observe a significant reduction in earthquake nucleation size due to δV_s . The theoretical equation for nucleation size in a layered medium (Kaneko et al., 2011) predicts that it should depend only on the shear modulus of the near-fault material given that other parameters are constant. This theoretical relationship overestimates the nucleation size observed in our models with precursors. We measure the nucleation size using the patch of the fault having higher slip-rate than the threshold velocity of 1 mm s⁻¹ at the start of the earthquakes. Fig. 2d shows that the nucleation size can be reduced by more than a half with increasing precursor duration for a constant 0.5% precursory velocity drop. This is seen across both $L_c = 2$ mm and $L_c = 8$ mm simulations. Additionally, since the slip-rate threshold used for setting

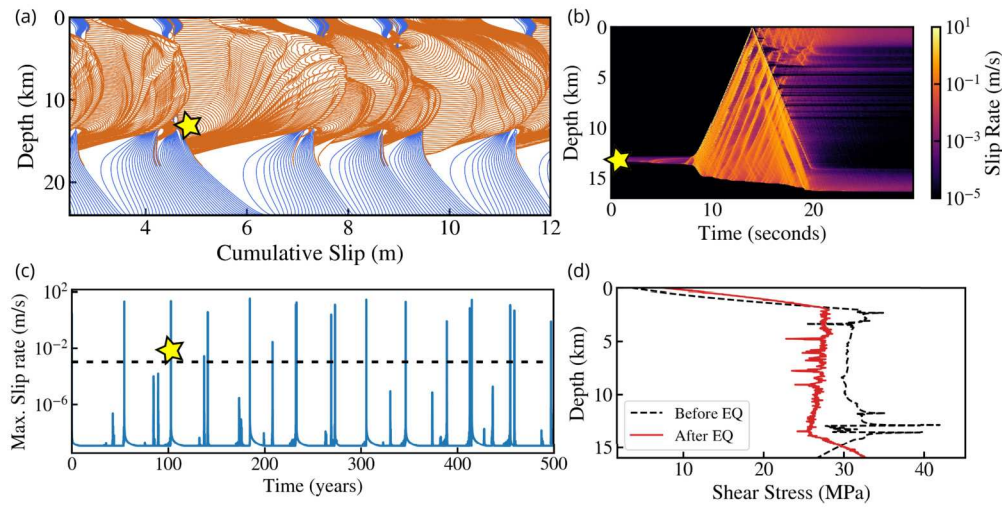


Fig. 3. Reference model with fault damage zone. (a) Cumulative slip through earthquake sequences shown along depth. The orange lines are plotted every 0.1 s during earthquakes, and the blue lines are plotted every two years during interseismic periods. (b) Spatiotemporal slip-rate for one representative large earthquake along depth and time. (c) The peak slip-rate on fault is shown in time, demonstrating a range of fast and slow events. The dashed line shows the seismic threshold. (d) The shear stress along depth before and after a representative earthquake. The yellow star shows the location of the representative earthquake highlighted in (b) and (d).

up the precursor onset duration cannot be lower than the background creep rate of $1 \times 10^{-9} \text{ m s}^{-1}$, the decrease in nucleation size will plateau as the precursor onset duration increases. Our results suggest that the nucleation size is also a function of precursory onset time, with a longer precursor duration leading to a smaller nucleation size.

3.2. Reference model: fully dynamic earthquake cycles with a fault damage zone

Our reference model consists of a fault-parallel damage zone extending throughout the depth of the domain, and a characteristic slip distance of $L_c = 2 \text{ mm}$. This reference model does not have any δV_s . However, the presence of damage zone, along with the prescribed nucleation size, gives rise to complexities in the earthquake sequence such as variability in earthquake magnitudes and hypocenter location as well as the presence of slow-slip events. These complexities result from a combination of stress heterogeneities generated by fault zone reflected waves during dynamic rupture (Harris and Day, 1997; Thakur et al., 2020) as well as multi-sized earthquake ruptures due to relatively small nucleation compared to the size of the fault asperity (Cattania, 2019; Barbot, 2019). The cumulative slip contours show that dynamic wave reflections affect seismic slip in large and small earthquakes (Fig. 3a). The spatiotemporal slip-rate of a representative earthquake (marked in yellow star) shown in Fig. 3b highlights multiple dynamic wave reflections, where parts of the fault have sub-seismic slip-rate ($< 1 \text{ mm s}^{-1}$) and other parts have seismic slip-rate. The rupture also propagates as slip pulses at any given depth. Additionally, our reference model has abundant slow-slip events between large earthquakes, as shown by the peak slip-rate along the fault in Fig. 3c. Fig. 3d shows the shear stress along the fault before and after the same earthquake. The shear stress before the earthquake highlights the overstressed nucleating region near 14 km depth. Furthermore, the shear stress after the earthquake is very heterogeneous in space, primarily because of dynamic wave reflections.

3.3. Effects of precursory velocity changes on earthquake cycles

We present four models with different precursory durations for $L_c = 2 \text{ mm}$ (Fig. 4a-d). The parameters used are listed in Table A.1, under Section 3.3. Increasing the precursory duration results in a higher number of large, surface-reaching events compared to our reference simulations. In Fig. 3a, the reference simulation shows one surface-reaching

event between 5-8 m slip, averaging one such event every 3 m of accumulated slip. Conversely, simulations with δV_s exhibit two or more surface-reaching events for every 3 m of accumulated slip (Fig. 4a-d). This surge in surface-reaching events is attributed to the introduction of δV_s , leading to faster and earlier nucleation of earthquakes.

Analyzing peak slip-rate in these simulations reveals that an earlier onset of δV_s corresponds to an earlier onset of earthquakes (Fig. 4e and f). The first earthquake in the reference model initiates at 55 yrs, while δV_s models exhibit earlier nucleation, synchronized with the precursor duration. Fig. 4f illustrates the onset of earthquakes and transient slow-slip events over time. The 30-day precursor model depicts two large earthquakes between 25 and 70 yrs, while the 1-hour, 2-day, and 20-day precursor models each feature one large earthquake in the same period. All simulations include one or more slow-slip transients during this time frame.

Both the 30-day precursor and the reference model experience fewer slow-slip transients between earthquakes than other precursor simulations. This indicates that if the precursor duration is sufficiently long, earthquake dynamics are closer to the reference model. The incorporation of precursory δV_s still influences earthquake onset, resulting in earlier nucleation in the 30-day precursor compared to the reference model. Simulations with precursors exhibit larger surface-reaching events and fewer small earthquakes due to accelerated earthquake nucleation triggered by precursory velocity-drops in the fault zone, leading to faster ruptures.

The size of earthquakes is also influenced by friction parameters L_c , as discussed in Section 3.4. Notably, the onset timing of the precursor does not directly correspond to how early the earthquake will nucleate. This is because we specify the duration of the velocity-drop in terms of the peak slip-rate, and fault slip begins accelerating as soon as the velocity-drop is specified.

We further examine the magnitude-frequency distribution and the depth distribution of earthquake hypocenters (Fig. 5). The earthquake magnitude is calculated by integrating fault slip over the rupture length for a given shear modulus within the fault zone, assuming the rupture width is equivalent to the rupture length in the 2D approximation. The cumulative magnitude-frequency distribution exhibits a sharp decline in the number of earthquakes beyond magnitude 6 and a log-linear trend for smaller ($M_w < 4$) earthquakes across all simulations. However, the reference simulation displays several intermediate magnitude earthquakes ($M_w 4-6$), with a log-linear decrease in the number of events

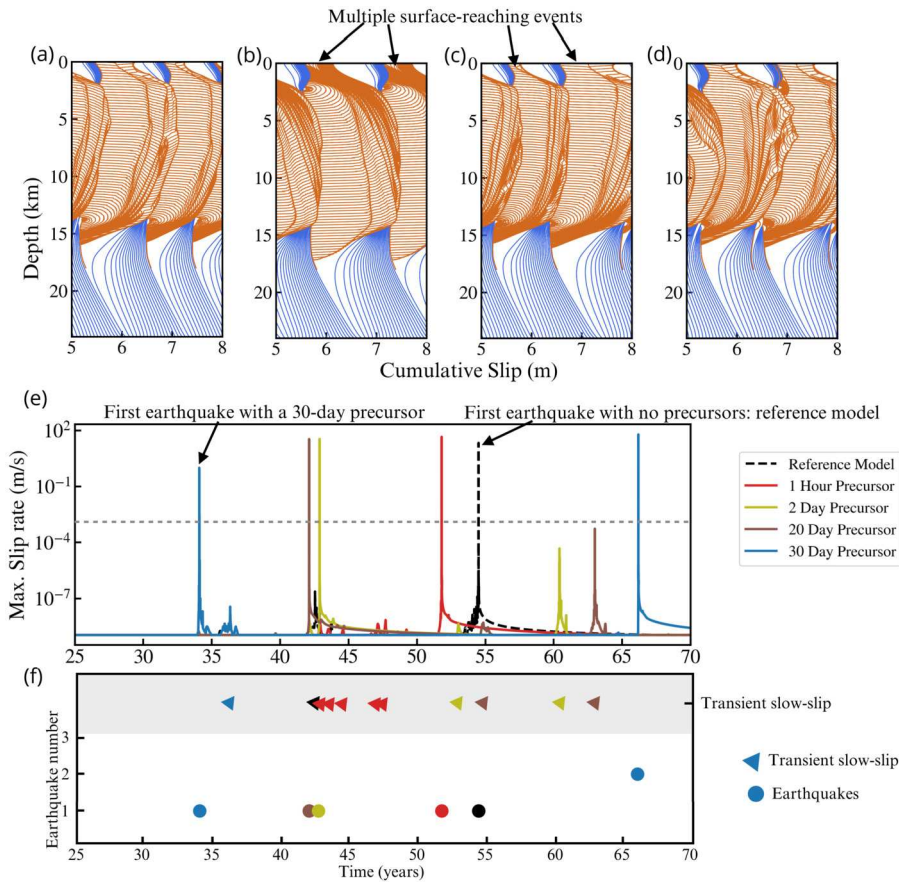


Fig. 4. A comparison of earthquake cycle models with different precursory velocity onset. (a-d) Cumulative slip for a section of the earthquake sequence for precursor onsets of (a) 1 hour, (b) 2 days, (3) 20 days, and (4) 30 days before earthquakes. The orange lines are plotted every 0.1 s and the blue lines are plotted every 1 yr. (e) Peak slip-rate on the fault shown in time for different precursor onsets and the reference simulation. The dashed gray line shows the seismic threshold. (f) Earthquakes and transient slow-slip against time shown for the set of simulations.

as magnitude increases, characterized by a distinct slope from smaller earthquakes. The gap in the intermediate magnitude earthquakes is present in all the precursor simulations, where the intermediate magnitude earthquakes happen as often as the reference simulation. This is also corroborated by the similarity in the depth distribution of earthquakes between the reference simulation and the 30-day precursor (Fig. 5b). The median hypocenter is closer to 15 km in the reference simulation and the simulation with δV_s of 1-hour, 20-day, and 30-day. The absolute deviation is however the largest for the reference simulation followed by the 30-day precursor. The δV_s for the other simulations have a very small absolute deviation of hypocenters. The simulation with 2-day precursor also has fewer total number of earthquakes compared to the other simulations (Fig. 5a), but the gap in intermediate magnitude earthquakes is still prevalent. This is because most earthquakes in this simulation occur at shallower depths, where it is harder for ruptures to stop without breaking through to the surface due to low fault strength at depths shallower than 5 km (Fig. 5b). Overall, this suggests that the impact of precursors on earthquake dynamics is stronger for shorter durations, and longer precursor durations may not significantly affect the occurrence of intermediate magnitude earthquakes. Despite these quantitative differences, our models are qualitatively similar in the sense that the incorporation of precursors causes a clock advance of earthquake nucleation, and disrupts the interplay between aseismic creep and dynamic earthquakes.

The earthquake hypocenter locations in the 20-day and 30-day precursor simulations show a higher degree of similarity to the reference simulation, with only a small difference in the distribution of hypocenters along depth (Fig. 5b). Specifically, the percentage of hypocenters located within a 5 km radius of the reference simulation increase from

65% in the 1-hour precursor simulation to 95% in the 20-day precursor simulation. Conversely, the 1-hour and 2-day precursors display a significant deviation from the reference simulation, with a noticeably different distribution of hypocenter depths. In particular, the shallow earthquakes in the 2-day precursor simulation result in a lower overall earthquake count compared to the other simulations (Fig. 5a). This observation is consistent with the fact that larger earthquakes are more likely to nucleate at the base of the seismogenic zone, which is not the case in the 2-day precursor simulation. Specifically, the percentage of large earthquakes (magnitude greater than 5) located within a 5 km radius of the reference simulation is only 20% in the 2-day precursor simulation, compared to 85% in the 30-day precursor simulation.

To understand the nucleation phase of these events with δV_s , we compare the spatiotemporal slip-rate history in our 20-day precursor simulation with our reference simulation. A comparison between Fig. 6a and Fig. 6b shows that we have fewer slow-slip events in the presence of velocity precursors. In other words, there is a lower number of earthquakes but a higher number of slow-slip events when there are no precursors. By zooming in to the nucleation phase, we find the incorporation of precursory velocity-drop results in a much shorter duration for the nucleation of earthquakes (Fig. 6c-d). In our simulation without precursors (Fig. 6c), the fault accelerates for 21 hours with peak fault slip-rate oscillating within the slow-slip regime ($< 1 \times 10^{-4} \text{ m s}^{-1}$) before growing into seismic event. In contrast, our simulation with δV_s (Fig. 6d) shows the nucleation phase acceleration for 3 hours before the seismic event, and the peak slip-rate oscillations are also fewer and restricted to less than 1 hour before the event. We see that while the largest magnitude surface-reaching earthquakes are comparable across the two simulations with the major difference being time-delay, there is

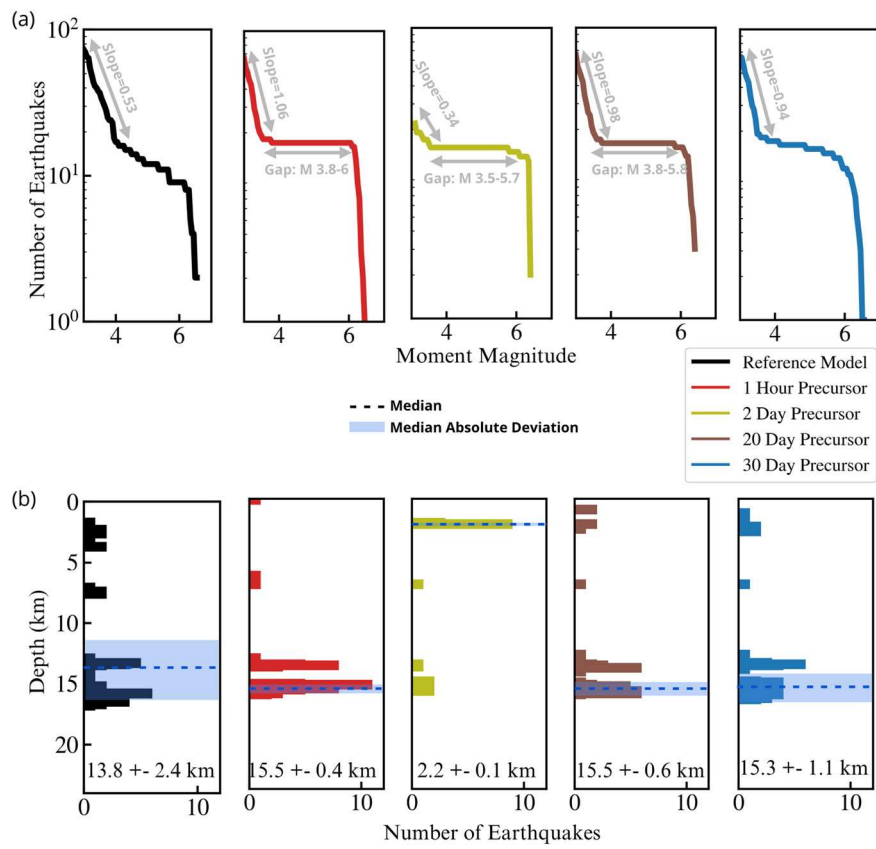


Fig. 5. (a) Magnitude-frequency distribution for our reference simulation and different precursor onset durations. (b) Depth distribution of earthquake hypocenters for the same simulations. The median and absolute deviation for the earthquakes is shown in dashed line and shaded region. The values are written at the bottom of the plot.

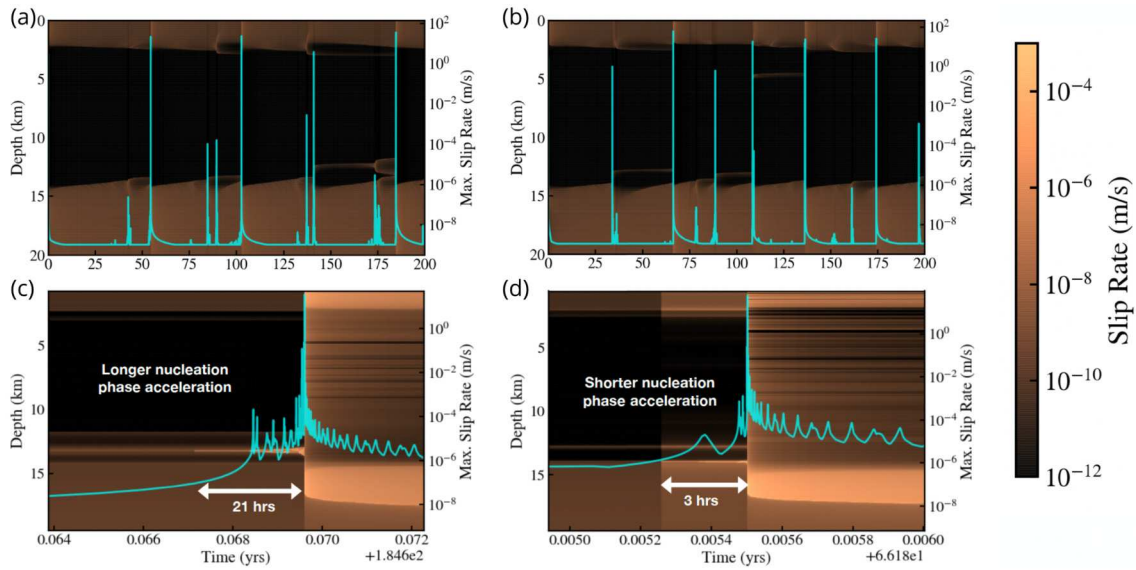


Fig. 6. a-c) Spatiotemporal slip-rate history of the reference simulation. (b-d) Spatiotemporal slip-rate history of the 20-day precursor. The bottom figures show the zoom-in of one representative earthquake from each simulation.

a dearth of certain slow-slip events and we have more number of larger earthquakes in our simulation with precursors (Fig. 6b).

3.4. Heterogeneous stress with and without precursors

Natural faults exhibit structural complexity, characterized by features like fault interface roughness, stress transfer from nearby faults,

and background stress heterogeneity (Smith and Heaton, 2011). Fault segments with varying shear stresses act as asperities facilitating rupture nucleation and propagation, while those with lower shear stresses act as barriers hindering rupture. The evolution of fault stress state, influenced by fault friction, geometry, and material properties, occurs through earthquake cycles and long-term interseismic slip.

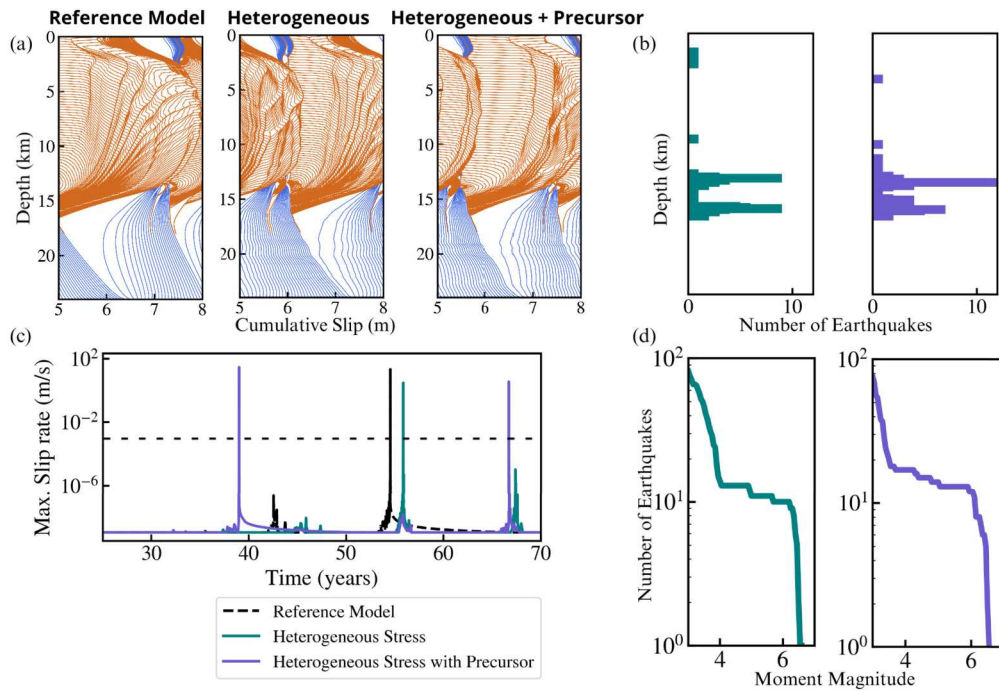


Fig. 7. Earthquake cycle simulations with self-similar (heterogeneous) initial normal stress. (a) A comparison of cumulative slip contours for three simulations: the reference model, the heterogeneous stress without precursors, and the heterogeneous stress with precursors. The orange lines are plotted every 0.1 s and the blue lines are plotted every 1 yr. (b) Depth distribution of earthquake hypocenters. (c) A comparison of peak slip-rate on the fault. The dashed line shows the seismic threshold. (d) Depth distribution of earthquake hypocenters. The magnitude-frequency and depth distribution of reference model are discussed in Fig. 4.

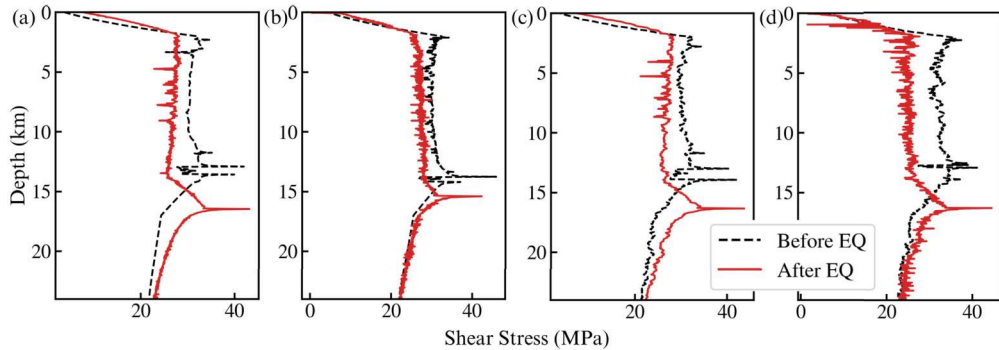


Fig. 8. Shear stress before and after one large earthquake. (a) Reference Simulation. (b) 20-Day Precursor. (c) Heterogeneous initial normal stress without precursor. (d) Heterogeneous initial normal stress with 20-day precursor.

To explore the persistence of δV_s effects in faults with prior stress heterogeneities, we simulate earthquake cycles incorporating self-similar normal stress distribution along depth, termed heterogeneous normal stress. Self-similarity refers to a property where a structure or phenomenon exhibits similar patterns or characteristics at different scales. Self-similarity is often observed in the patterns of stress changes within fault systems (e.g., (Smith and Heaton, 2011)). This means that the stress changes at various scales within the fault exhibit similarities, allowing researchers to apply consistent modeling principles across different magnitudes and stages of earthquakes. The concept of self-similarity is valuable in understanding and predicting earthquake behaviors, aiding in the development of models that can capture the complexity of seismic processes across a range of scales. Using a one-dimensional stochastic, fractal-like model for heterogeneous stress (Smith and Heaton, 2011), we analyze its impact alongside velocity precursors and a fault damage zone.

The incorporation of self-similar normal stress affects earthquake nucleation size (Rubin and Ampuero, 2005; Kaneko et al., 2011), introducing variability with depth. The simulation with heterogeneous nor-

mal stress displays a rough slip profile for the aseismic part, in contrast to the reference model showing a rough coseismic slip profile (Fig. 7a). While the heterogeneous normal stress model delays earthquake nucleation compared to the reference model (Fig. 7c), the introduction of δV_s (20 days prior to the earthquake) leads to earlier nucleation, akin to results in Fig. 4. Figs. 7b and d illustrate the magnitude-frequency distribution and depth distribution of earthquake hypocenters for simulations with heterogeneous normal stress. While more earthquakes nucleate near the base of the seismogenic zone compared to the reference model (Fig. 4), the overall distribution appears similar between models with and without δV_s . This suggests that, although δV_s strongly influences earthquake nucleation onset, its impact on earthquake size and depth distribution is weaker than the effects of the fault damage zone structure, heterogeneous normal stress, and frictional parameters.

Comparing shear stresses before and after a representative earthquake between simulations with and without δV_s and initial heterogeneous normal stress (Fig. 8), the reference simulation with the fault damage zone exhibits post-earthquake heterogeneous shear stress within the seismogenic zone (2 km to 17 km in Fig. 8a). Stress hetero-

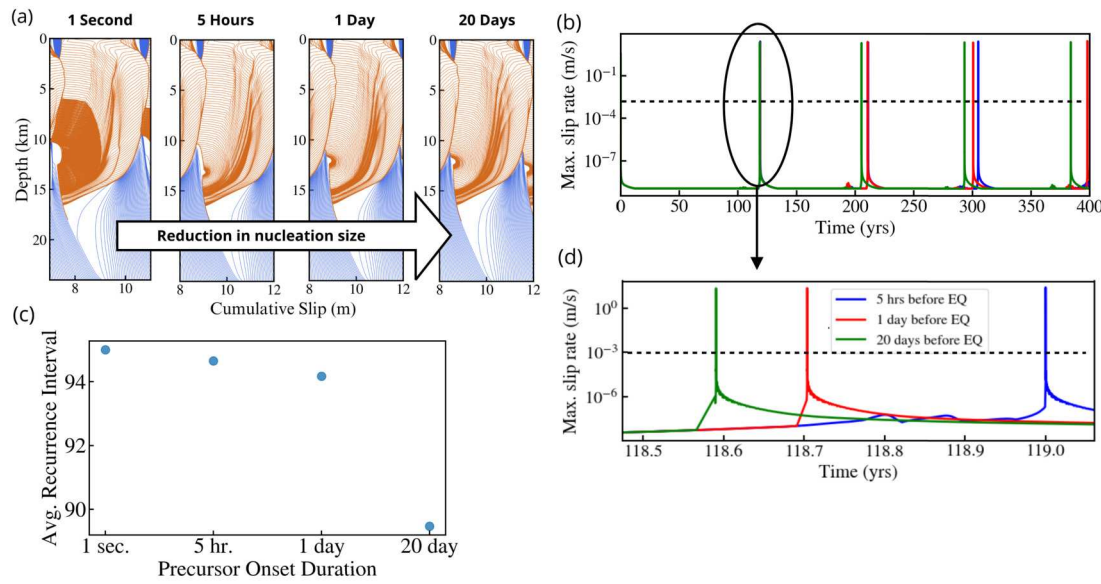


Fig. 9. (a) Cumulative slip profiles for simulations with different precursor onset durations. The orange lines are plotted every 0.1 s and the blue lines are plotted every 1 yr. (b) A comparison of peak slip-rate on the fault for three precursor durations. (c) Precursor onset duration shown against average recurrence intervals. (d) Zoom-in of Fig. 9b showing the earlier nucleation of earthquakes with earlier precursor onset times. The dashed lines show the seismic threshold.

genetics are caused by dynamic wave reflections, limited to the region of rupture propagation. The shear stress before an earthquake lacks heterogeneities, except for stress peaks near the nucleation region and the frictional transition boundary. While the location and number of these peaks in the reference simulation are influenced by stress heterogeneities from previous earthquakes, they are not present at every point along the fault, unlike subsequent simulations.

With the inclusion of δV_s (Fig. 8b), shear stress before the earthquake becomes heterogeneous within the seismogenic zone. Additional initial heterogeneous normal stress results in creeping regions of the fault exhibiting shear stress heterogeneities, amplified in the presence of velocity precursors (Figs. 8c and d).

3.5. δV_s change with a larger nucleation size ($L_c = 8$ mm)

In this section, we carry out more simulations using $L_c = 8$ mm while keeping the other parameters similar as the above sections. The larger L_c results in a proportionately larger nucleation size and therefore periodic, full ruptures are exclusively observed in these simulations. The parameters used are listed in Table A.1, under Section 3.5. Fig. 9a shows the cumulative slip for four simulations with different precursor duration. We see a clear reduction in nucleation size as the precursor duration increases and thus earlier earthquake rupture onsets (Figs. 9b and d). The incorporation of such δV_s also results in a log-linear acceleration of slip-rate as discussed previously (Fig. 9d). However, the reduction in nucleation size for $L_c = 8$ mm does not cause additional earthquake complexities such as small earthquakes and variable hypocenter locations. We note that the material and frictional properties are the same across these simulations, therefore the reduction in nucleation size is caused solely due to the onset of precursory velocity-drop. The simulation with δV_s 1 s before the earthquake also shows a very slow rupture propagation during the start of rupture, demonstrated by very dense cumulative slip contours during the seismic event (Fig. 9a). Additionally, across all these simulations, the earthquake magnitude remains unchanged for these large, periodic events. Since our models are two-dimensional, the earthquake magnitude predominantly depends on the rupture length along the dip-direction. Our results show that δV_s does not contribute to any change in rupture length for large periodic events, however, the magnitude of earthquakes along natural faults may be affected by the rupture width along the strike direction. An analysis of the average recurrence interval against

the precursor duration is shown in Fig. 9c. We see a direct decrease in the recurrence interval between two large earthquakes as the precursor onset duration increases. If there is a long period of precursor activity before a large earthquake, then the time between that earthquake and the next one is likely to be shorter than if there was a shorter precursor period. This suggests that the length and intensity of the precursor activity can be used to estimate the onset of subsequent large earthquake.

4. Discussion and conclusions

In this study, we have explored the impact of precursory velocity changes on earthquake dynamics, particularly focusing on their influence on earthquake nucleation size, surface-reaching events, hypocenter distribution, and recurrence intervals. Notably, we observed a significant reduction in earthquake nucleation size, independent of substantial alterations in elastic material properties in section 3.5. This reduction manifested in changes to the occurrence of surface-rupturing large events and the distribution of earthquake hypocenters. Furthermore, we delved into the temporal aspects, investigating how varying the precursor onset duration affects earthquake onset time and recurrence.

Fig. 10 shows the earthquake magnitudes for our simulations with different precursor durations with $L_c = 2$ mm. We can see how the earthquake magnitude changes through time, and that the reference model has the most variability. The largest magnitude events are surface-rupturing and extend through the entire fault width. There is a gap in intermediate magnitude earthquakes and we have some smaller earthquakes in all these simulations. The 2-day precursor has a lack of smaller magnitude earthquakes. As the precursor duration increases and reaches the 30-day duration, we see that there are more intermediate magnitude earthquakes and the catalog is in close resemblance to the reference model. The magnitude-frequency distribution of earthquakes usually follows a power-law relationship, best described by the Gutenberg-Richter (G-R) distribution. Most observations of global and regional seismicity agree with the G-R distribution (Page and Felzer, 2015; Rundle, 1989). However, certain observations of magnitude-frequency distributions along more planar faults (e.g., the San Andreas Fault) have shown a “characteristic earthquake” distribution, wherein the largest earthquake of a characteristic size recurs with an approximately regular interval. The period between two such characteristic

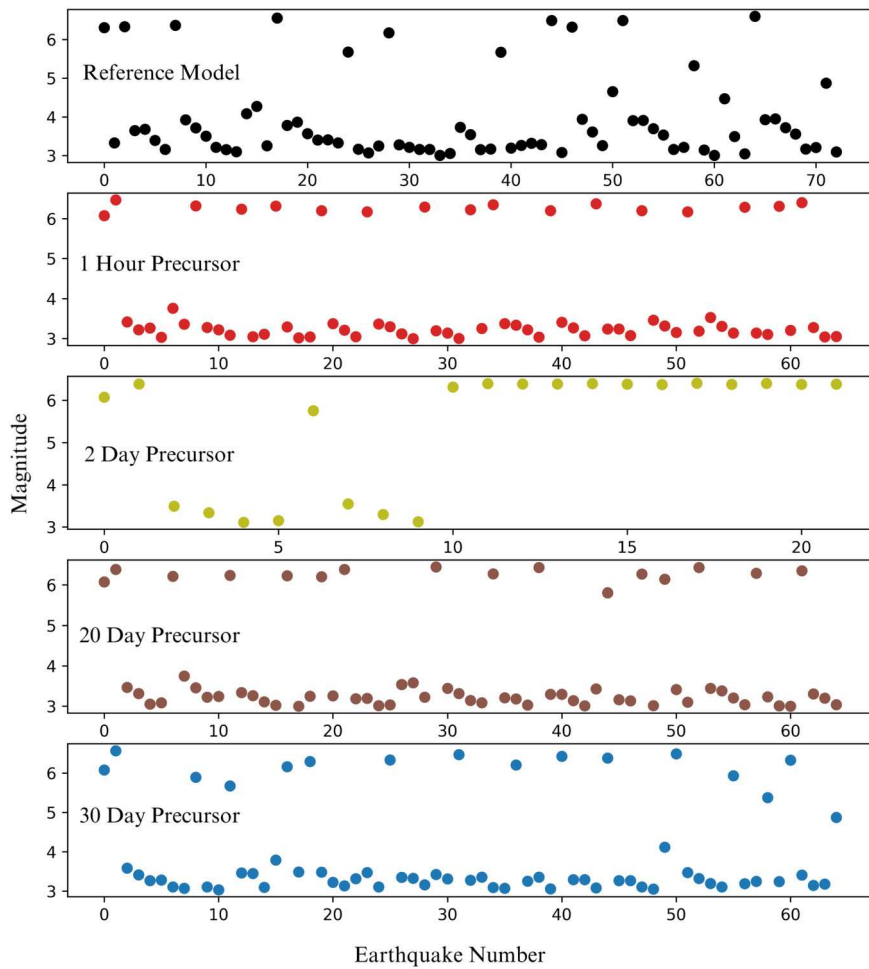


Fig. 10. Magnitude and event number of earthquakes for precursor models with $L_c = 2$ mm, shown for different precursor durations.

earthquakes is generally quiescent except for low-level seismic activity (Schwartz and Coppersmith, 1984; Wesnousky, 1994). While our reference simulation shows a more log-linear decrease of earthquake size, the simulations with precursory velocity changes are more akin to a characteristic distribution with a dearth of intermediate magnitude earthquakes (Fig. 5a, 7d). Despite the similarities, the slope of the distribution is different from what is observed in nature, primarily due to our choice of friction parameters and the two-dimensional model approximations. Since the effective normal stress and hence the fault strength is low at depths shallower depths, it is harder to stop dynamic ruptures once they reach this shallow depth. When the rupture breaks through the free surface, the magnitude of the earthquakes tends to be much larger, which, in combination with a lack of along-strike rupture termination, may explain the lack of certain range of intermediate magnitude earthquakes (Thakur et al., 2020). Despite these shortcomings, our models can be potentially linked to well monitored strike slip fault systems like the Parkfield segment, where the current consensus of delay of cyclic earthquakes is attributed to the creeping segments acting as barriers and the local stress heterogeneities from surrounding fault systems (Bakun et al., 2005; Barbot et al., 2009).

Our study has focused on imposing precursors and self-similar stresses under an elastic approximation to study their effects on earthquake cycles. However, we have not considered the physical mechanisms that may be responsible for such material properties and stress changes through the earthquake cycle, e.g., incorporating plasticity (Erickson and Dunham, 2014; Mia et al., 2022) or continuum damage rheology (Lyakhovsky et al., 1997; Thomas and Bhat, 2018) within the fault damage zone. Incorporation of inelastic behavior in the fault zone

promotes the accumulation of permanent deformation throughout the fault zone evolution. Such deformation may lead to a complex feedback between the evolving fault zone medium and seismic events, generating unique off-fault rupture patterns (Thomas and Bhat, 2018) and self-consistent healing and damage accumulation (Lyakhovsky et al., 1997). Mia et al. (2022) have shown that the off-fault plastic accumulation may lead to partial ruptures and clustering of seismic events in time. In our simulations, these mechanisms will likely affect the slow-slip generation during the aseismic phase and modulate the shear stress evolution throughout the seismic cycle. Additionally, due to the huge computational costs, we have not explored the detailed parameter space for the choice of damage zone geometry as well as precursory velocity onset and amplitude, which are likely to reveal additional fault zone physics in relation to the velocity precursors. Despite these approximations in our study, our simulations with prescribed precursory velocity drop before the earthquake highlight the importance of monitoring such velocity changes in natural faults, which can potentially aid in seismic hazard assessment.

In conclusion, we present two-dimensional, fully dynamic earthquake cycle simulations with an elastic fault damage zone and analyze the effects of precursory velocity changes with variable onset durations. We further investigate the effects of additional apriori stress heterogeneities with and without such precursory velocity changes. Our models demonstrate that the earthquake nucleation size is reduced by more than half due to a precursory velocity change of 0.5%, depending on how early this change occurs prior to the earthquake. This implies that the earthquake nucleation size can be significantly smaller than those predicted from theoretical equations (Rubin and Ampuero, 2005)

if the shear modulus, effective normal stress, and frictional parameters vary temporally during the earthquake preparation phase. Furthermore, compared to a reference scenario without any precursory velocity drop, earthquakes can nucleate earlier in the seismic cycle, with earlier precursor onset resulting in earlier earthquake onset. Despite this significant reduction in earthquake nucleation time, we find that the magnitude of earthquakes is comparable across different models for our simulations with $L_c = 8$ mm, whereas they can be highly variable for simulations with $L_c = 2$ mm, suggesting that the complexities in earthquake sequences also depend on fault frictional parameters such as the characteristic slip distance L_c . Our models also highlight the relative effects of heterogeneous stress evolution in the presence of fault damage zones and precursory velocity reductions. Fault stress heterogeneities generated by rupture in fault damage zones can affect the rupture nucleation and propagation of future earthquakes. However, the incorporation of preexisting self-similar stresses promotes the heterogeneous distribution of stresses during both rupture propagation and aseismic creep. For homogeneous initial stress conditions, precursory velocity changes affect earthquake statistics like the magnitude-frequency distribution and the hypocenter location, while for a heterogeneous initial stress condition, earthquake statistics are not affected significantly. Studies like Scuderi et al. (2016) have shown that precursory change in seismic velocity has been observed in a spectrum of earthquake failure modes, including tremor and low-frequency earthquakes. We have modeled the precursory changes prior to large earthquakes, and shown that it can lead to a disruption in the recurrence of large earthquakes, favoring an advance in the earthquake onset. Subsequently, a delay in the onset of earthquakes can be caused by such disruption if slow-slip and accelerated creep events occur on fault between such large earthquakes. Seismicity observations along the Parkfield segment of San Andreas fault have shown such disruption in periodic seismicity of the regular recurring events (Bakun et al., 2005), attributed to the unique creeping segment along the fault and to the local stress changes from the surrounding fault systems. Our study can provide additional mechanisms, in a purely elastic assumption, for such disruptions. By exploring a range of complexities due to precursory velocity drop and heterogeneous normal stresses, our dynamic earthquake cycle models suggest that more detailed and frequent observations of natural fault zones can help us better understand the aperiodicity of earthquakes along strike-slip fault systems.

CRediT authorship contribution statement

Prithvi Thakur: Writing – original draft, Visualization, Software, Methodology, Formal analysis. **Yihe Huang:** Writing – review & editing, Supervision, Methodology, Investigation, Funding acquisition, Conceptualization.

Declaration of competing interest

The authors declare that they have no known competing financial interests or personal relationships that could have appeared to influence the work reported in this paper.

Data availability

No data was used for the research described in the article.

Acknowledgements

This study was supported by the National Science Foundation (Grant Award EAR-1943742) and Southern California Earthquake Center (Contribution number 20091).

Appendix A

Table A.1
Parameters Used in Numerical Simulations of Earthquake Cycles.

Parameter	Symbol	Value
Static friction coefficient	μ_0	0.6
Reference velocity	V_0	$1 \times 10^{-6} \text{ m s}^{-1}$
Plate loading rate	V_{pl}	35 mm yr^{-1}
Evolution effect	b	0.019
Effective normal stress	σ	50 MPa
Initial shear stress	τ_0	30 MPa
Steady-state velocity dependence	$(b-a)$	-0.004
Width of seismogenic zone	W	10 km
Fault damage zone width	W_d	0.5 km
Average node spacing	dx	20 m
Seismic slip rate threshold	V_{th}	1 mm s^{-1}
Shear modulus of host rock	μ	32 GPa
Shear modulus of damage zone	μ_D	15.7 GPa
Shear modulus after the velocity drop	$\mu_{\delta V_s}$	14.9 GPa
Section 3.3		
Characteristic weakening distance	L_c	2 mm
Precursory velocity threshold (onset duration 1 hr)	Vf_{thresh}	$8 \times 10^{-4} \text{ m s}^{-1}$
Precursory velocity threshold (onset duration 2 day)	Vf_{thresh}	$1 \times 10^{-8} \text{ m s}^{-1}$
Precursory velocity threshold (onset duration 20 day)	Vf_{thresh}	$5 \times 10^{-9} \text{ m s}^{-1}$
Precursory velocity threshold (onset duration 30 day)	Vf_{thresh}	$2 \times 10^{-9} \text{ m s}^{-1}$
Section 3.5		
Characteristic weakening distance	L_c	8 mm
Precursory velocity threshold (onset duration 1 sec)	Vf_{thresh}	$9.9 \times 10^{-4} \text{ m s}^{-1}$
Precursory velocity threshold (onset duration 5 hrs)	Vf_{thresh}	$9 \times 10^{-7} \text{ m s}^{-1}$
Precursory velocity threshold (onset duration 1 day)	Vf_{thresh}	$1 \times 10^{-8} \text{ m s}^{-1}$
Precursory velocity threshold (onset duration 20 day)	Vf_{thresh}	$5 \times 10^{-9} \text{ m s}^{-1}$

References

Abdelmeguid, M., Ma, X., Elbanna, A., 2019. A novel hybrid finite element-spectral boundary integral scheme for modeling earthquake cycles: application to rate and state faults with low-velocity zones. *J. Geophys. Res., Solid Earth*.

Andrews, D.J., Barall, M., 2011. Specifying initial stress for dynamic heterogeneous earthquake source models. *Bull. Seismol. Soc. Am.* 101, 2408–2417. <https://doi.org/10.1785/0120110012>.

Andrews, D.J., Ma, S., 2016. Validating a dynamic earthquake model to produce realistic ground motion. *Bull. Seismol. Soc. Am.* 106, 665–672. <https://doi.org/10.1785/0120150251>.

Bakun, W., Aagaard, B., Dost, B., Ellsworth, W.L., Hardebeck, J.L., Harris, R.A., Ji, C., Johnston, M.J., Langbein, J., Lienkaemper, J.J., et al., 2005. Implications for prediction and hazard assessment from the 2004 Parkfield earthquake. *Nature* 437, 969–974.

Barbot, S., 2019. Slow-slip, slow earthquakes, period-two cycles, full and partial ruptures, and deterministic chaos in a single asperity fault. *Tectonophysics* 768, 228171.

Barbot, S., Fialko, Y., Bock, Y., 2009. Postseismic deformation due to the mw 6.0 2004 Parkfield earthquake: stress-driven creep on a fault with spatially variable rate-and-state friction parameters. *J. Geophys. Res., Solid Earth* 114.

Blanpied, M., Lockner, D., Byerlee, J., 1991. Fault stability inferred from granite sliding experiments at hydrothermal conditions. *Geophys. Res. Lett.* 18, 609–612.

Bouchon, M., Durand, V., Marsan, D., Karabulut, H., Schmittbuhl, J., 2013. The long precursory phase of most large interplate earthquakes. *Nat. Geosci.* 6 (4), 299–302. <https://doi.org/10.1038/ngeo1770>. <https://www.nature.com/articles/ngeo1770>.

Cattania, C., 2019. Complex earthquake sequences on simple faults. *Geophys. Res. Lett.* 46, 10384–10393.

Chiarabba, C., De Gori, P., Segou, M., Cattaneo, M., 2020. Seismic velocity precursors to the 2016 mw 6.5 Norcia (Italy) earthquake. *Geology* 48, 924–928.

Cicerone, R.D., Ebel, J.E., Britton, J., 2009. A systematic compilation of earthquake precursors. *Tectonophysics* 476, 371–396.

Cox, S., Scholz, C., 1995. Experimental deformation of fault gouge. *J. Struct. Geol.* 17, 1–15.

Dalguer, L.A., Mai, P.M., 2011. Near-source ground motion variability from M~6.5 dynamic rupture simulations, IASPEI and IAEE. <https://www.research-collection.ethz.ch/handle/20.500.11850/43732>. (Accessed 9 June 2017).

Dieterich, J.H., 1979. Modeling of rock friction: 1. experimental results and constitutive equations. *J. Geophys. Res., Solid Earth* 84, 2161–2168. <https://doi.org/10.1029/JB084iB05p02161>. <https://agupubs.onlinelibrary.wiley.com/doi/abs/10.1029/JB084iB05p02161>. <https://agupubs.onlinelibrary.wiley.com/doi/pdf/10.1029/JB084iB05p02161>.

Ellsworth, W., Beroza, G., 1995. Seismic evidence for an earthquake nucleation phase. *Science* 268, 851–855.

Erickson, B.A., Dunham, E.M., 2014. An efficient numerical method for earthquake cycles in heterogeneous media: alternating subbasin and surface-rupturing events on faults crossing a sedimentary basin. *J. Geophys. Res., Solid Earth* 119, 3290–3316.

Erickson, B.A., Jiang, J., Barall, M., Lapusta, N., Dunham, E.M., Harris, R., Abrahams, L.S., Allison, K.L., Ampuero, J.P., Barbot, S., et al., 2020. The community code verification exercise for simulating sequences of earthquakes and aseismic slip (seas). *Seismol. Res. Lett.* 91, 874–890.

Harris, R.A., Day, S.M., 1997. Effects of a low-velocity zone on a dynamic rupture. *Bull. Seismol. Soc. Am.* 87, 1267–1280.

Huang, Y., Ampuero, J.P., 2011. Pulse-like ruptures induced by low-velocity fault zones. *J. Geophys. Res., Solid Earth* 116. <https://doi.org/10.1029/2011JB008684>. <https://agupubs.onlinelibrary.wiley.com/doi/abs/10.1029/2011JB008684>. <https://agupubs.onlinelibrary.wiley.com/doi/pdf/10.1029/2011JB008684>.

Huang, Y., Ampuero, J.P., Helmberger, D.V., 2014. Earthquake ruptures modulated by waves in damaged fault zones. *J. Geophys. Res., Solid Earth* 119, 3133–3154.

Hulbert, C., Rouet-Leduc, B., Johnson, P.A., Ren, C.X., Rivière, J., Bolton, D.C., Marone, C., 2019. Similarity of fast and slow earthquakes illuminated by machine learning. *Nat. Geosci.* 12 (1), 69–74. <https://doi.org/10.1038/s41561-018-0272-8>. <https://www.nature.com/articles/s41561-018-0272-8>.

Ito, Y., Hino, R., Suzuki, S., Kaneda, Y., 2015. Episodic tremor and slip near the Japan Trench prior to the 2011 Tohoku-Oki earthquake. *Geophys. Res. Lett.* 42, 1725–1731. <https://doi.org/10.1002/2014GL062986>. <https://onlinelibrary.wiley.com/doi/abs/10.1002/2014GL062986>. <https://onlinelibrary.wiley.com/doi/pdf/10.1002/2014GL062986>.

Kaneko, Y., Ampuero, J.P., Lapusta, N., 2011. Spectral-element simulations of long-term fault slip: effect of low-rigidity layers on earthquake-cycle dynamics. *J. Geophys. Res., Solid Earth* 116, B10313. <https://doi.org/10.1029/2011JB008395>.

Kato, A., Nakagawa, S., 2014. Multiple slow-slip events during a foreshock sequence of the 2014 Iquique, Chile Mw 8.1 earthquake. *Geophys. Res. Lett.* 41, 5420–5427. <https://doi.org/10.1002/2014GL061138>. <https://onlinelibrary.wiley.com/doi/abs/10.1002/2014GL061138>. <https://onlinelibrary.wiley.com/doi/pdf/10.1002/2014GL061138>.

Kato, A., Obara, K., Igarashi, T., Tsuruoka, H., Nakagawa, S., Hirata, N., 2012. Propagation of slow slip leading up to the 2011 Mw 9.0 Tohoku-Oki earthquake. *Science* 335, 705–708. <https://doi.org/10.1126/science.1215141>. <https://www.science.org/doi/full/10.1126/science.1215141>.

Lapusta, N., Rice, J.R., 2003. Nucleation and early seismic propagation of small and large events in a crustal earthquake model. *J. Geophys. Res., Solid Earth* 108. <https://doi.org/10.1029/2001JB000793>. <https://onlinelibrary.wiley.com/doi/abs/10.1029/2001JB000793>. <https://onlinelibrary.wiley.com/doi/pdf/10.1029/2001JB000793>.

Lapusta, N., Rice, J.R., Ben-Zion, Y., Zheng, G., 2000. Elastodynamic analysis for slow tectonic loading with spontaneous rupture episodes on faults with rate- and state-dependent friction. *J. Geophys. Res., Solid Earth* 105, 23765–23789. <https://doi.org/10.1029/2000JB00250>. <https://agupubs.onlinelibrary.wiley.com/doi/abs/10.1029/2000JB00250>. <https://agupubs.onlinelibrary.wiley.com/doi/pdf/10.1029/2000JB00250>.

Lewis, M.A., Ben-Zion, Y., 2010. Diversity of fault zone damage and trapping structures in the Parkfield section of the San Andreas fault from comprehensive analysis of near fault seismograms. *Geophys. J. Int.* 183, 1579–1595.

Lyakhovsky, V., Ben-Zion, Y., Agnon, A., 1997. Distributed damage, faulting, and friction. *J. Geophys. Res., Solid Earth* 102, 27635–27649. <https://doi.org/10.1029/97JB01896>. <https://onlinelibrary.wiley.com/doi/abs/10.1029/97JB01896>. <https://onlinelibrary.wiley.com/doi/pdf/10.1029/97JB01896>.

Mendecki, A., Chester, F., 2000. Fault zone architecture and the evolution of deformation bands. *J. Struct. Geol.* 22, 457–474.

Mia, M.S., Abdelmeguid, M., Elbanna, A.E., 2022. Spatio-temporal clustering of seismicity enabled by off-fault plasticity. *Geophys. Res. Lett.* 49, e2021GL097601.

Nanjo, K.Z., Hirata, N., Obara, K., Kasahara, K., 2012. Decade-scale decrease in b value prior to the M9-class 2011 Tohoku and 2004 Sumatra quakes. *Geophys. Res. Lett.* 39. <https://onlinelibrary.wiley.com/doi/abs/10.1029/2012GL052997>. <https://onlinelibrary.wiley.com/doi/pdf/10.1029/2012GL052997>.

Nie, S., Barbot, S., 2021. Seismogenic and tremorigenic slow slip near the stability transition of frictional sliding. *Earth Planet. Sci. Lett.* 569, 117037. <https://doi.org/10.1016/j.epsl.2021.117037>. <https://www.sciencedirect.com/science/article/pii/S0012821X21002922>.

Niu, F., Silver, P.G., Daley, T.M., Cheng, X., Majer, E.L., 2008. Preseismic velocity changes observed from active source monitoring at the Parkfield SAFOD drill site. *Nature* 454, 7201. <https://doi.org/10.1038/nature07111>. <https://www.nature.com/articles/nature07111>.

Osawa, S.W., Hatano, T., Kame, N., 2019. Longer migration and spontaneous decay of aseismic slip pulse caused by fault roughness. *Geophys. Res. Lett.* 46, 636–643. <https://doi.org/10.1029/2018GL081465>. <https://onlinelibrary.wiley.com/doi/abs/10.1029/2018GL081465>. <https://onlinelibrary.wiley.com/doi/pdf/10.1029/2018GL081465>.

Page, M., Felzer, K., 2015. Southern San Andreas fault seismicity is consistent with the Gutenberg–Richter magnitude–frequency distributions southern San Andreas fault seismicity is consistent with the Gutenberg–Richter magnitude–frequency distribution. *Bull. Seismol. Soc. Am.* 105, 2070. <https://doi.org/10.1785/0120140340>. <https://gsw/content/public/journal/bssa/105/4/10.1785/0120140340/3/2070.pdf>.

Perrin, C., Manighetti, I., Ampuero, J.P., Cappa, F., Gaudemer, Y., 2016. Location of largest earthquake slip and fast rupture controlled by along-strike change in fault structural maturity due to fault growth. *J. Geophys. Res., Solid Earth* 121, 3666–3685. <https://doi.org/10.1002/2015JB012671>. <https://agupubs.onlinelibrary.wiley.com/doi/pdf/10.1002/2015JB012671>.

Poli, P., 2017. Creep and slip: seismic precursors to the nuugaatsiaq landslide (Greenland). *Geophys. Res. Lett.* 44, 8832–8836. <https://doi.org/10.1002/2017GL075039>. <https://onlinelibrary.wiley.com/doi/abs/10.1002/2017GL075039>. <https://onlinelibrary.wiley.com/doi/pdf/10.1002/2017GL075039>.

Ripperger, J., Ampuero, J.P., Mai, P.M., Giardini, D., 2007. Earthquake source characteristics from dynamic rupture with constrained stochastic fault stress. *J. Geophys. Res., Solid Earth* 112. <https://doi.org/10.1029/2006JB004515>. <https://onlinelibrary.wiley.com/doi/abs/10.1029/2006JB004515>. <https://onlinelibrary.wiley.com/doi/pdf/10.1029/2006JB004515>.

Rivet, D., De Barros, L., Guglielmi, Y., Cappa, F., Castilla, R., Henry, P., 2016. Seismic velocity changes associated with aseismic deformations of a fault stimulated by fluid injection. *Geophys. Res. Lett.* 43, 9563–9572. <https://doi.org/10.1002/2016GL070410>. <https://onlinelibrary.wiley.com/doi/abs/10.1002/2016GL070410>. <https://onlinelibrary.wiley.com/doi/pdf/10.1002/2016GL070410>.

Rubin, A., Ampuero, J.P., 2005. Earthquake nucleation on (aging) rate and state faults. *J. Geophys. Res., Solid Earth* 110.

Ruina, A., 1983. Slip instability and state variable friction laws. *J. Geophys. Res., Solid Earth* 88, 10359–10370. <https://doi.org/10.1029/JB088iB12p10359>. <https://agupubs.onlinelibrary.wiley.com/doi/pdf/10.1029/JB088iB12p10359>. <https://agupubs.onlinelibrary.wiley.com/doi/abs/10.1029/JB088iB12p10359>.

Rundle, J.B., 1989. A physical model for earthquakes: 3. thermodynamical approach and its relation to nonclassical theories of nucleation. *J. Geophys. Res., Solid Earth* 94, 2839–2855. <https://doi.org/10.1029/JB094iB03p02839>. <https://agupubs.onlinelibrary.wiley.com/doi/pdf/10.1029/JB094iB03p02839>. <https://agupubs.onlinelibrary.wiley.com/doi/abs/10.1029/JB094iB03p02839>.

Scholz, C.H., 1998. Earthquakes and friction laws. *Nature* 391, 37–42.

Schwartz, D.P., Coppersmith, K.J., 1984. Fault behavior and characteristic earthquakes: examples from the Wasatch and San Andreas fault zones. *J. Geophys. Res., Solid Earth* 89, 5681–5698. <https://doi.org/10.1029/JB089iB07p05681>. <https://agupubs.onlinelibrary.wiley.com/doi/pdf/10.1029/JB089iB07p05681>. <https://agupubs.onlinelibrary.wiley.com/doi/abs/10.1029/JB089iB07p05681>.

Scuderi, M.M., Marone, C., Tinti, E., Di Stefano, G., Colletti, C., 2016. Precursory changes in seismic velocity for the spectrum of earthquake failure modes. *Nat. Geosci.* 9, 695–700. <https://doi.org/10.1038/ngeo2775>. <https://www.nature.com/articles/ngeo2775>. bandiera_abtest: a Cg_type: Nature Research Journals Number: 9 Primary_atype: Research Publisher: Nature Publishing Group Subject_term: Natural hazards; Seismology; Tectonics Subject_term_id: natural-hazards; seismology; tectonics.

Shreedharan, S., Bolton, D.C., Rivière, J., Marone, C., 2020. Preseismic fault creep and elastic wave amplitude precursors scale with lab earthquake magnitude for the continuum of tectonic failure modes. *Geophys. Res. Lett.* 47, e2020GL086986.

Sibson, R., 1977. Fault Rocks and Fault Mechanisms. Wiley.

Smith, D.E., Heaton, T.H., 2011. Models of stochastic, spatially varying stress in the crust compatible with focal-mechanism data, and how stress inversions can be biased toward the stress rate. *Bull. Seismol. Soc. Am.* 101, 1396–1421.

Stanchits, S.A., Lockner, D.A., Ponomarev, A.V., 2003. Anisotropic changes in P-wave velocity and attenuation during deformation and fluid infiltration of granite. *Bull. Seismol. Soc. Am.* 93, 1803–1822. <https://doi.org/10.1785/0120020101>.

Tal, Y., Hager, B.H., 2018. Dynamic mortar finite element method for modeling of shear rupture on frictional rough surfaces. *Comput. Mech.* 61, 699–716. <https://doi.org/10.1007/s00466-017-1475-3>.

Tal, Y., Hager, B.H., Ampuero, J.P., 2018. The effects of fault roughness on the earthquake nucleation process. *J. Geophys. Res., Solid Earth* 123, 437–456. <https://doi.org/10.1002/2017JB014746>. <https://onlinelibrary.wiley.com/doi/abs/10.1002/2017JB014746>.

Thakur, P., Huang, Y., 2021. Influence of fault zone maturity on fully dynamic earthquake cycles. *Geophys. Res. Lett.* 48, e2021GL094679.

Thakur, P., Huang, Y., Kaneko, Y., 2020. Effects of low-velocity fault damage zones on long-term earthquake behaviors on mature strike-slip faults. *J. Geophys. Res., Solid Earth* 125. <https://doi.org/10.1029/2020JB019587>. <https://onlinelibrary.wiley.com/doi/10.1029/2020JB019587>.

Thomas, M.Y., Bhat, H.S., 2018. Dynamic evolution of off-fault medium during an earthquake: a micromechanics based model. *Geophys. J. Int.* 214, 1267–1280. <https://doi.org/10.1093/gji/ggy129>.

Thurber, C., Roecker, S., Roberts, K., Gold, M., Powell, L., Rittger, K., 2003. Earthquake locations and three-dimensional fault zone structure along the creeping section of the San Andreas fault near Parkfield, CA: preparing for SAFOD. *Geophys. Res. Lett.* 30. <https://doi.org/10.1029/2002GL016004>. <https://onlinelibrary.wiley.com/doi/abs/10.1029/2002GL016004>. <https://onlinelibrary.wiley.com/doi/pdf/10.1029/2002GL016004>.

Vidale, J.E., Li, Y.G., 2003. Damage to the shallow landers fault from the nearby hector mine earthquake. *Nature* 421, 524–526.

Wesnousky, S.G., 1994. The Gutenberg–Richter or characteristic earthquake distribution, which is it? *Bull. Seismol. Soc. Am.* 84, 1940. <https://doi.org/10.1785/0120140340>.

pubs.geoscienceworld.org/ssa/bssa/article-abstract/84/6/1940/119861/The-Gutenberg-Richter-or-characteristic-earthquake.

Whitcomb, J.H., Garmany, J.D., Anderson, D.L., 1973. Earthquake prediction: variation of seismic velocities before the San Francisco earthquake. *Science* 180, 632–635. <https://doi.org/10.1126/science.180.4086.632>. <https://www.science.org/doi/abs/10.1126/science.180.4086.632>.

Yang, H., Zhu, L., Cochran, E.S., 2011. Seismic structures of the Calico fault zone inferred from local earthquake travel time modelling. *Geophys. J. Int.* 186, 760–770. <https://doi.org/10.1111/j.1365-246X.2011.05055.x>.